CHEMISTRY OF MATERIALS
Article

Chem. Mater. **2010,** *22,* 957–965 957
DOI:10.1021/cm901875u

Correlation of Fuel Cell Anode Electrocatalytic and ex situ Catalytic Activity of Perovskites $La_{0.75}Sr_{0.25}Cr_{0.5}X_{0.5}O_{3-\delta}$ (X = Ti, Mn, Fe, Co)†

Nemanja Danilovic,‡ Adrien Vincent,‡ Jing-Li Luo,*,‡ Karl T. Chuang,‡ Rob Hui,§ and Alan R. Sanger‡

‡*Department of Chemical and Materials Engineering, University of Alberta, ECERF Building 7-084H, 107−116 Street, Edmonton, AB, Canada T6G 2 V4, and* §*NRC Institute for Fuel Cell Innovation, 4250 Wesbrook Mall, Vancouver, B.C. V6T 1W5*

Received June 29, 2009. Revised Manuscript Received September 25, 2009

The performance of a series of perovskite oxides having the mutual chemical formula and structure $La_{0.75}Sr_{0.25}Cr_{0.5}X_{0.5}O_{3-\delta}$ (X = Co, Fe, Ti, Mn) as solid oxide fuel cell anode electrocatalysts depends on the nature of the substituent element X. The electrocatalytic activity for methane oxidation in a fuel cell correlates well with ex-situ temperature programmed catalytic conversion of CH_4, X = Co > Mn ∼ Fe > Ti, under temperature programmed reaction conditions in 5% CH_4/He. The total conductivity of the materials in air decreases X = Co > Fe > Mn > Ti. Within the series of catalysts, the order of maximum fuel cell power density depended on feed: CH_4, X = Fe > Mn > Ti; H_2, X = Fe > Mn > Ti; and 0.5% H_2S/CH_4, X = Ti > Fe > Mn. The Co-containing catalyst was unstable under reducing conditions. A process is proposed to explain the difference in catalyst order and enhanced activities in H_2S/CH_4 as fuel compared to CH_4 alone.

1.0. Introduction

Solid oxide fuel cells (SOFCs) are electrochemical devices that directly convert the chemical energy of a fuel into electrical energy. The overall reaction is separated into oxidation of a fuel on the anode catalyst and reduction of oxygen at the cathode catalyst, separated by an impermeable oxygen ion conducting electrolyte. In principle, a variety of fuels can be used and, through selection of appropriate materials, there can be high tolerance to impurities in the feeds. However, in practice, pure hydrogen is used to take advantage of the high catalytic reactivity of catalysts such as Ni.[1−3] However, H_2 fuel is produced from CH_4 and/or H_2O,[4] and the preferred Ni catalysts are intolerant to even small amounts of S-containing impurities that may be present, thus requiring expensive purification of H_2.

Similarly, direct use of impure hydrocarbon fuels as feed over conventional $Ni-Zr_{0.92}Y_{0.08}O_2$ (YSZ, 8% ytrria stabilized zirconia) anode catalysts results in contamination (H_2S poisoning) and degradation (carbon deposition).[5] A more economical and technically preferable alternative is a SOFC anode catalyst that can utilize CH_4 directly and which is tolerant of impurities such as H_2S.[6,7] To operate efficiently for a commercially viable lifetime, such an anode catalyst must satisfy the following requirements: high CH_4 electro-oxidation activity, sulfur tolerance, coking resistance, redox stability, and high electronic and ionic conductivity.[7]

Herein, we will show that the catalytic and electrocatalytic performance for conversion of H_2, CH_4, and CH_4/0.5% H_2S, of a series of catalysts having a common perovskite structure depends on the elemental composition of perovskites $La_{0.75}Sr_{0.25}Cr_{0.5}X_{0.5}O_{3-\delta}$ (LSCX; X = Co, Fe, Ti, Mn), in which X occupies the B site. The series of perovskites having Cr in the B site was selected as it was expected that Cr would impart redox stability to all of the structures.[8−10] They are each mixed conductors, although they are primarily electronic conductors, hence they are not ideal for use as single phase electrode materials. To improve applicability, they can be used in a composite anode with an ionic conducting component (such as gadolinia doped ceria or YSZ).

The LSCX perovskites containing Mn, Fe, and Ti are known, but have not been comparatively tested to establish trends across the 3d-series transition metal cations

† Accepted as part of the 2010 "Materials Chemistry of Energy Conversion Special Issue".

*E-mail: Jingli.Luo@ualberta.ca. Tel.: 1(780)492-2232. Fax: 1(780)492-2881.

(1) Sun, C.; Stimming, U. *J. Power Sources* **2007**, *171*, 247.
(2) Minh, N. Q. *Solid State Ionics* **2004**, *174*, 271.
(3) Singhal, S. C., Kendall, K., Eds. *High Temperature Solid Oxide Fuel Cells: Fundamentals, Design, and Applications*; Elsevier: New York, 2003.
(4) Edwards, P. P.; Kuznetsov, V. L.; David, W. I. F. *Phil. Trans. R. Soc. A.* **2007**, *365*, 1043.
(5) Offer, G. J.; Mermelstein, J.; Brightman, E.; Brandon, N. P. *J. Am. Ceram. Soc.* **2009**, *92*, 763.
(6) Gong, M.; Liu, X.; Trembly, J.; Johnson, C. *J. Power Sources* **2007**, *168*, 289.
(7) Gross, M. D.; Vohs, J. M.; Gorte, R. J. *J. Mater. Chem.* **2007**, *17*, 3071.
(8) Konysheva, E; Irvine, J. T. S. *Chem. Mater.* **2009**, *21*, 1514.
(9) Sfeir, J. *J. Power Sources* **2003**, *118*, 276.
(10) Nowotny, J., Sorrell, C. C., Eds. *Key Engineering Materials*; Trans Tech Publications: Switzerland, 1997; Vol. *125−126*, p 187.

Published on Web 10/21/2009

upon which to form bases for any selection for electrocatalytic applications.[11−18] In addition, a Co-containing perovskite, LSCCo, was tested as a potentially catalytically active material within the group LSCX wherein X is selected from the first row D-series elements. It is known that $Ce_{0.9}Sr_{0.1}Cr_{0.5}V_{0.5}O_{3-\delta}$ is relatively inactive for conversion of CH_4 which is why we did not perform further tests using the LSCV perovskite.[19,20] Although $La_{0.7}Sr_{0.3}VO_3$ has recently been reported as being active, its redox stability is known to be inadequate.[19,21] Ni, and Cu containing perovskites are known to be unstable at low oxygen partial pressures, leading to segregation of the metal.[22−24] The present research was directed to determination of the relative catalytic activity of this family of perovskites, to provide data for rational development of future materials selection for SOFC anode materials.

We also describe a rapid technique using simultaneous differential scanning calorimetry−thermogravimetric analysis−mass spectrometry (DSC-TGA-MS) for screening potential candidate catalysts for CH_4 activity and carbon deposition resistance in an environment closely simulating anode fuel cell conditions.[17,18,24−26] We then demonstrate its utility by comparing the present series of perovskites for catalytic and electrocatalytic CH_4 conversion and stability in 5000 ppm H_2S.

2.0. Experimental Section

2.1. Catalyst Preparation. LSC and LSCX catalyst powders were prepared using combustion gel synthesis. Initially, stoichiometric amounts of the nitrates $La(NO_3)_3 \cdot 6H_2O$ (Alfa Aesaer, 99.9%), $Sr(NO_3)_2$ (Alfa Aesaer, 99%), $Co(NO_3)_2 \cdot 6H_2O$ (Sigma Aldrich, 98%), $Fe(NO_3)_3 \cdot 9H_2O$ (BDH, 98%), $Mn(NO_3)_2$ solution (Alfa Aesaer, 99%), $Cr(NO_3)_3 \cdot 9H_2O$ (Acros Organics, 99%), $Ce(NO_3)_3 \cdot 6H_2O$ (Acros Organics, 99.5%), and $Gd(NO_3)_3 \cdot 6H_2O$ (Sigma Aldrich, 99.9%) were mixed in water. The mixture was stirred continuously on a hot plate at ~90 °C. Citric acid was added to form a 2:1 ratio of acid to metal cations. Ammonium hydroxide (Fisher Scientific) was added to balance the pH to ~7. The mixture was stirred further on the hot plate at 90 °C for several hours until the water had evaporated. The temperature was increased to 100 °C to form a gel. Once the gel was formed, the beaker was placed directly into a combustion furnace at 500 °C. After 30 min, the temperature was increased to 600 °C and held at that value for 1 h to combust all carbonaceous material from the mixture. The porous foams that formed were ground using a mortar and pestle and then calcined in air at 1000 °C for 4 h. The resulting powders were dispersed in isopropanol then milled overnight in a ZrO_2 ball mill with ZrO_2 balls. LSCTi was prepared via a different procedure using titanium isopropoxide (Sigma Aldrich, 98%). Chromium deficient $La_{0.75}Sr_{0.25}Cr_{0.5}Q_{0.5}O_{3-\delta}$ (Q representing a missing B site cation) was prepared by the gel combustion process above and the resulting powder was dispersed in distilled water and stirred to form a suspension at 80 °C, into which the stoichiometric amount of titanium isopropoxide was injected. The resulting solution was dried and ground before calcining in air at 1000 °C for 4 h.

Investigation of the potential utility of the present catalysts was extended by preparation and testing of composite catalysts combining the benefits of additional components having complementary activity with that of the substituted perovskites. Composite $Ce_{0.9}Gd_{0.1}O_2$ (GDC)−LSCX catalysts in 50/50 mass ratio were milled for 24 h.

2.2. Temperature Programmed Analysis. Temperature programmed analyses were conducted using simultaneous DSC-TGA-MS using a TA Instruments SDT Q600 connected to a mass spectrometer (Pfeiffer Thermostar GSD 301). The two instruments were connected by a transfer line maintained at 200 °C. The following reactions were performed sequentially on catalyst powders: oxidation in 5% O_2/He, reduction in 1% H_2/He, reoxidation in 5% O_2/He, temperature programmed reaction (TPR) with methane in 5% CH_4/He, and temperature programmed oxidation (TPO) in 5% O_2/He. A flow rate of 100 mL min^{-1} was used in all experiments, except for the reaction in CH_4/He where a flow rate of 500 mL min^{-1} was utilized to minimize the effect of gas phase thermal reactions. An accurately measured sample of about 5 mg of powder was placed in an alumina cup (90 μL), then the system was purged for 30 min using 100 mL min^{-1} flowing He prior to testing. The samples were then heated to 1000 at 20 °C min^{-1}. The samples were not exposed to air between tests.

2.3. Conductivity Testing. Conductivity measurements were conducted using a NorECs Probostat electrochemical measurement cell in atmospheres that were either air or 5% H_2/Ar. Cylindrical pellets were prepared by pressing powdered catalyst at 2 tonnes in a 1 cm i.d. die and sintering for 2 h at the following temperatures: LSCFe, 1400 °C; LSCCo, 1350 °C; LSCTi, 1550 °C; and LSCMn, 1400 °C. The samples were heated at 2 °C min^{-1} to prescribed temperatures of 500−950 °C at which tests were performed. The samples were held at testing temperature until the conductivity value was stable. The measurements were performed using the four-point van der Pauw DC technique using platinum point contacts.

2.4. Fuel Cell Testing. MEAs having the configuration LSCX|YSZ (0.3 mm)|Pt were prepared, installed, and tested in the fuel cell testing apparatus shown in a previous publication.[19] Au paint was applied to the anode as a current collector and sintered in situ. The anode and cathode chamber gas flow rates were each 100 mL min^{-1}, and the chamber volume was close to 80 mL, so the residual time of the gases was about 0.8 min.

Membrane electrode assemblies (MEA) were tested at each temperature, 800, 850, and 900 °C, consecutively. The fuels used for testing were varied in the following order H_2, CH_4, and 0.5% H_2S/CH_4. The cells were held at open circuit voltage (OCV) for at least 30 min after switching fuels or changing temperature and for 5−10 min after each potentiodynamic and impedance test.

(11) Pudmich, G.; Boukamp, B. A.; Gonzalez-Cuenca, M.; Jungen, W.; Zipprich, W.; Tietz, F. *Solid State Ionics* **2000**, *135*, 433.
(12) Tsipis, E. V.; Kharton, V. V. *J. Solid State Electroch.* **2008**, *12*, 1367.
(13) Tao, S.; Irvine, J. T. S. *Nat. Mater.* **2003**, *2*, 320.
(14) Tao, S.; Irvine, J. T. S. *Chem. Mater.* **2004**, *16*, 4116.
(15) Fisher, J. C.; Chuang, S. S. C. *Catal. Commun.* **2009**, *10*, 772.
(16) Rossmeisl, J.; Bessler, W. G. *Solid State Ionics* **2008**, *178*, 1694.
(17) Bruce, M. K.; van den Bossche, M.; McIntosh, S. *J. Electrochem. Soc.* **2008**, *155*, B1202.
(18) van den Bossche, M.; McIntosh, S. *J. Catal.* **2008**, *255*, 313.
(19) Danilovic, N; Luo, J. L.; Chuang, K. T.; Sanger, A. R. *J. Power Sources* **2009**, *192*, 247.
(20) Danilovic, N; Luo, J. L.; Chuang, K. T.; Sanger, A. R. *J. Power Sources* **2009**, *194*, 252–262.
(21) Ge, X. M.; Chanz, S. H. *J. Electrochem. Soc.* **2009**, *156*, B386.
(22) Nakamura, T.; Petzow, G.; Gauckler, L. J. *Mater. Res. Bul.* **1979**, *14*, 649.
(23) Falcon, H.; Martinez-Lope, M. J.; Alonso, J. A.; Fierro, J. L. G. *Appl. Catal., B* **2000**, *26*, 131.
(24) Baker, R. T.; Metcalfe, I. S. *Appl. Catal., A* **1995**, *126*, 319.
(25) Baker, R. T.; Metcalfe, I. S. *Ind. Eng. Chem. Res.* **1995**, *34*, 1558.
(26) Baker, R. T.; Metcalfe, I. S. *Appl. Catal., A* **1995**, *126*, 297.

Potentiostatic tests at an uncompensated cell voltage of 0.7 V were conducted at 850 °C for 6 h for each MEA following completion of the sequence of potentiodynamic tests and then cooling the cell from 900 to 850 °C and holding it at that temperature.

2.5. Materials Characterization. A Rigaku RU200 powder X-ray diffraction (XRD) system with a rotating anode and a Co target was used for analysis of all synthesized powders, with a scan rate of $2\,^{\circ}\theta\,\mathrm{min}^{-1}$. The commercially available software Jade was used for identification of phases in the samples. A Hitachi S-4800 field emission scanning electron microscope (SEM) was used for characterizing cross sections of MEAs. Quantachrome Instruments Autosorb I was used for Brunauer−Emmett−Teller (BET) surface area determination of freshly prepared catalysts. Elemental analyses using inductively coupled plasma-MS (ICP-MS) were conducted utilizing a Perkin-Elmer Elan 6000 and solutions prepared by digesting the powders in a mixture of nitric and hydrochloric acids at 125 °C. A Setaram Setsys Evolution dilatometer was used to determine the thermal expansion coefficients (TEC) of samples in flowing air.

3.0. Results

3.1. Materials Characterization. The XRD patterns of the prepared oxide powders (Figure 1) showed that all of the synthesized materials possessed perovskite structures with a tetragonal unit cell, similar to that of the $LaCrO_3$ parent (PDF no. 24-1016). The dimensions of the unit cells were similar and varied with the size of the cation X (Table 1). The XRD patterns contained double peaks at high diffraction angles which were generated by the use of unfiltered $K\alpha_2$ X-rays. The BET surface areas of all the oxides were similar and high compared to powders prepared by conventional solid state synthesis. The TEC for each of LSCX (X = Mn, Fe) was compatible with that of YSZ and, therefore, unlikely to cause fracturing of the MEA through differential thermal expansion. However, LSCCo had a much larger TEC value than that of YSZ, used as electrolyte, and caused the anode to delaminate from the YSZ disk upon cooling of the sintered MEA. LSCTi was not tested in the dilatometer; however, experimentally there were no issues with TEC.

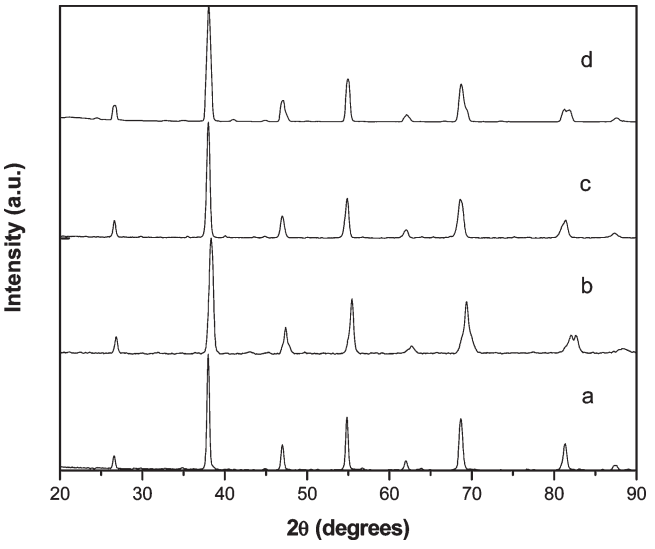

Figure 1. XRD patterns of (a) LSCFe, (b) LSCTi, (c) LSCCo, and (d) LSCMn prepared by gel synthesis.

SEM images of cross sections of LSCFe anodes (Figure 2) showed that the anode adhered well to the YSZ electrolyte after sintering. Anode catalyst particles were well-dispersed, well-interconnected, and the structure had good porosity. LSCMn and LSCTi were similarly well-adhered and had similar porosity.

Electronic transport characterization showed that the conductivities of tested materials were in the order LSCCo > LSCFe > LSCMn > LSCTi in both air and hydrogen. All of these anode materials were mixed conductors. LSCCo was reduced in H_2, and this caused the pellet to crack, as detailed below. All materials, except for LSCCo, had total conductivity sufficiently high that they were suitable candidates for testing for anode catalyst applications. Table 1 compares the activation energies and conductivities for all tested anode materials at 800 °C, and the Arrhenius plots are shown in Figure 3.

Of all the materials tested, only LSCCo was reduced in the 2% H_2/Ar stream, and peaks for Co metal were present in the XRD spectrum of reduced material. There were no secondary phases detectable using XRD following heating of 50/50 wt % mixtures of LSCX−YSZ (1200 °C, 6 h) air or in 2% H_2/Ar.

3.2. Temperature Programmed Analysis. The MS data during TPR for all of the catalysts is shown in Figure 4, and the corresponding TGA and DSC data (acquired simultaneously) are in Figures 5 and 6. The TPR data showed that the order of catalytic activity or methane oxidation (based on the normalized CO_2 evolved; Table 2) is LSCCo > LSCMn ~ LSCFe > LSCTi. The CO_2 MS signals indicated initial deep methane oxidation in which lattice oxygen reacted with methane, after which H_2 was formed concurrently with the onset of carbon deposition after all readily available lattice oxygen was spent. The oxidation of methane correlated directly with the reduction in mass of the samples through loss of oxygen (TGA, Figure 5), and the oxidation reaction was evident as corresponding DSC peaks (Figure 6). No similar DSC peak was present in the test using LSCTi, no CO_2 was formed, and the weight of the LSCTi sample remained constant, indicating that LSCTi had no significant activity for oxidation of CH_4. In contrast, each of LSCCo, LSCFe and LSCMn was an active oxidizer.

Table 1. Summary of Anode Materials' Properties

material	LSCTi	LSCMn	LSCFe	LSCCo
elemental comp ICP	$La_{0.73}Sr_{0.26}Cr_{0.45}Ti_{0.55}O_3$	$La_{0.82}Sr_{0.18}Cr_{0.44}Mn_{0.56}O_3$	$La_{0.80}Sr_{0.20}Cr_{0.50}Fe_{0.50}O_3$	$La_{0.80}Sr_{0.20}Cr_{0.48}Co_{0.52}O_3$
BET surface area/$m^2\ g^{-1}$	5.22	4.28	5.61	3.60
σ_{total} (Air/H_2 @ 800 °C)/S cm^{-1}	$1.37 \times 10^{-2}/3.95 \times 10^{-3}$	$1.75/2.22 \times 10^{-1}$	5.73/6.45	133.58/NA
E_a (Air/H_2)/eV	0.72/0.91	0.53/0.68	0.64/0.49	0.39/NA
TEC (K^{-1})	NA	$10.8 \times 10^{-6\,25}$	11.8×10^{-6}	19.5×10^{-6}

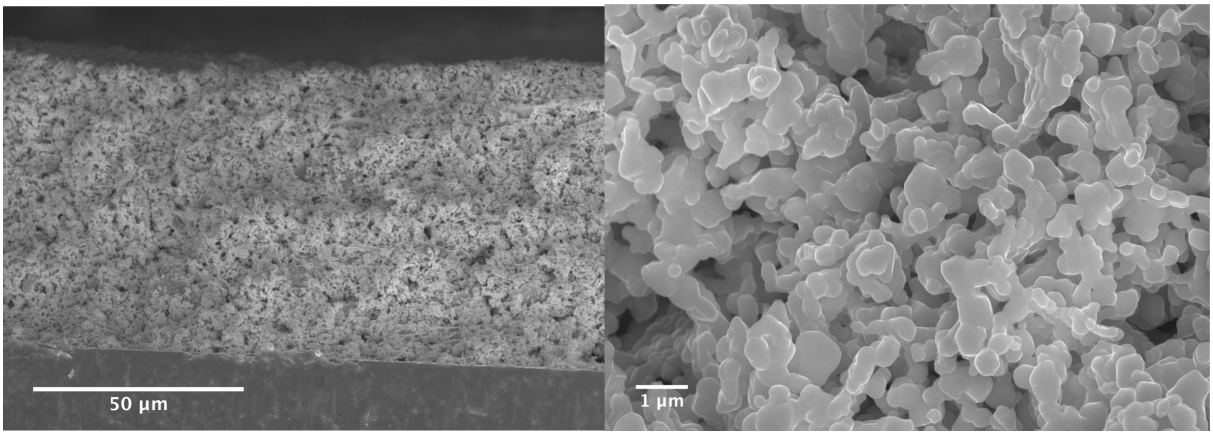

Figure 2. Cross-sectional SEM micrographs of prepared MEAs of LSCFe.

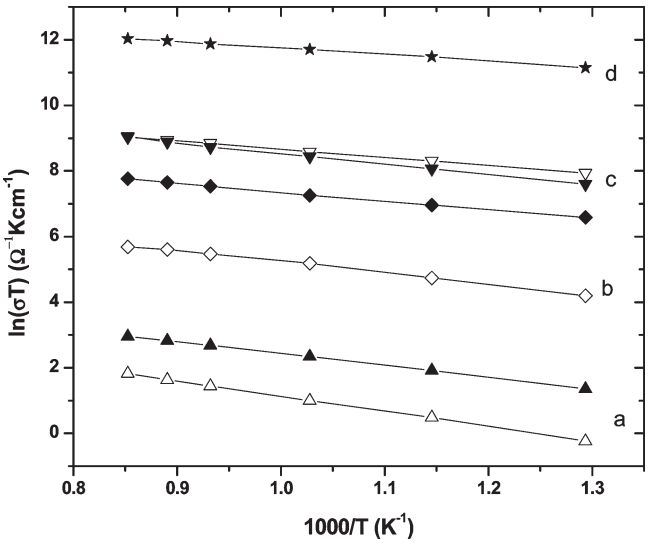

Figure 3. Conductivity comparison for (a) LSCTi, (b) LSCMn, (c) LSCFe, and (d) LSCCo in air (full symbols) and humidified 5% H_2 (clear symbols).

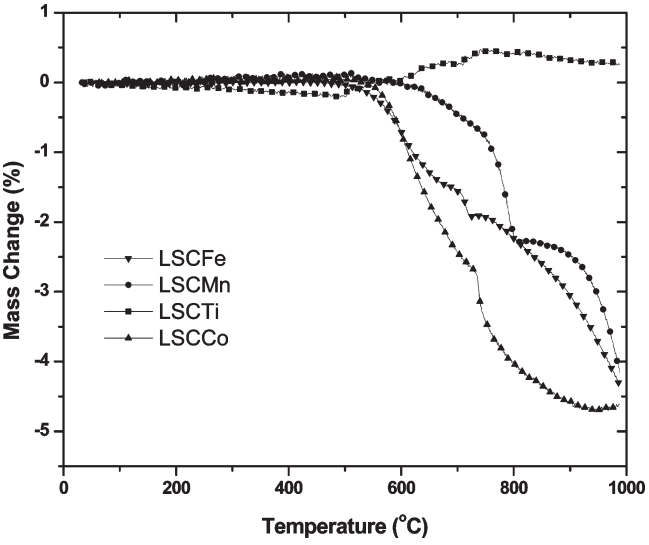

Figure 4. TGA data during TPR of oxide anode materials in 5% CH_4.

After all available surface O was depleted, carbonaceous deposits were formed on all of the materials during

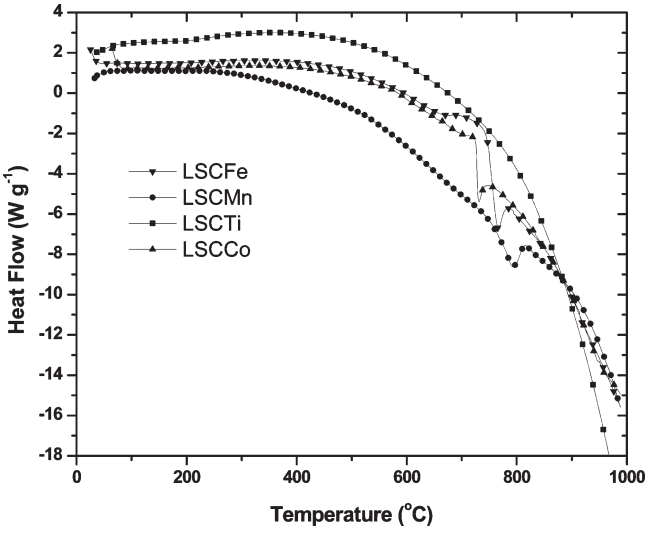

Figure 5. DSC data during TPR of oxide anode materials in 5% CH_4.

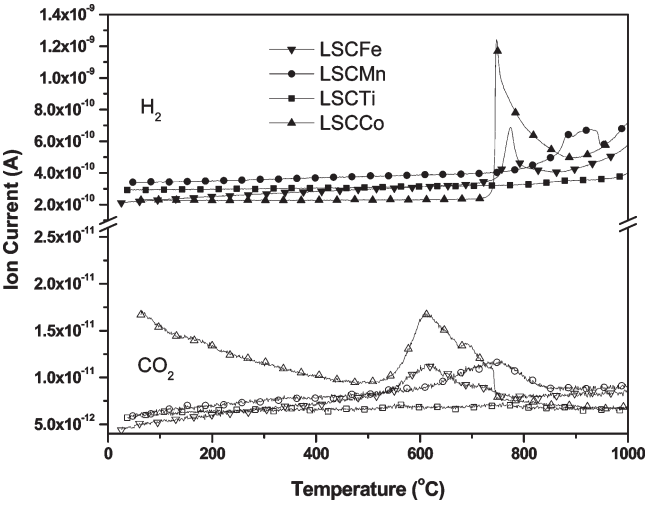

Figure 6. MS data during TPR of oxide anode materials in 5% CH_4.

prolonged heating under flowing CH_4−He, When the materials were then heated in air CO_2 was formed, providing a quantitative measure of the carbon deposited (Figure 7). When the deposited carbonaceous deposits included both C and H, there were also H_2O evolution

Table 2. Normalized CO_2 Evolution during TPR of CH_4 with LSCX

	CO_2 evolved (Ag °C^{-1} m^{-2})
LSCTi	NA
LSCMn	8.73×10^{-11}
LSCFe	6.74×10^{-11}
LSCCo	6.20×10^{-10}

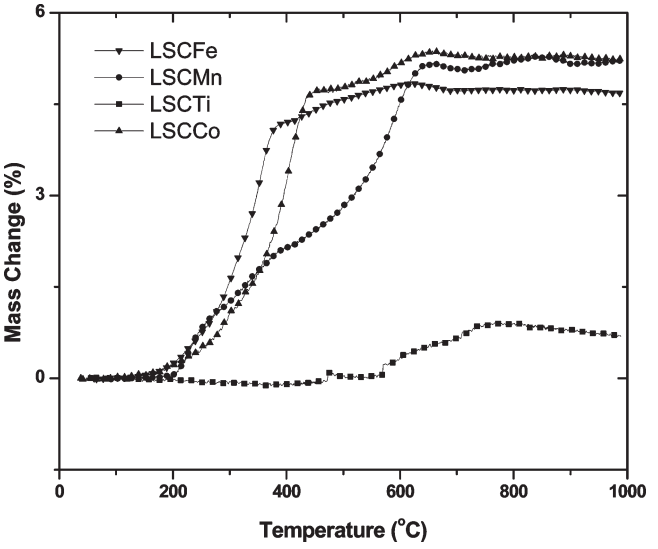

Figure 7. TGA data during TPO of oxide anode materials in 5% O_2.

Table 3. Normalized CO_2 Evolution during TPO of Carbonaceous Deposits with O_2

	CO_2 evolved (Ag °C^{-1} m^{-2})
LSCTi	8.74×10^{-10}
LSCMn	1.43×10^{-9}
LSCFe	1.18×10^{-9}
LSCCo	3.98×10^{-9}

peaks. The amount of deposited carbon was similar for all tested materials, and the temperatures for onset of evolution of CO_2 were each in the range 400−600 °C (Table 3). Only reactions of CH_4−He over LSCCo and LSCFe formed C- and H-containing carbonaceous deposits, which then gave rise to H_2O evolution starting at about 225 °C and occurring in two stages. TGA and DSC curves (Figures 8 and 9) showed that all of the materials that were reduced under CH_4−He were reoxidized fully during TPO.

3.3. Electrochemical Characterization. Initial electrocatalytic tests were conducted using each LSCX as single component anodes, even though this is not anticipated to provide optimal performance, so as to ascertain their independent catalytic contributions. Later, GDC was added as a second phase to form composite anodes and so improve the ionic conductivity.

Typical potentiodynamic performance curves are shown in Figure 10 for a fuel cell using LSCFe at 850 °C, and the corresponding impedance spectra for all materials, temperatures, and gases used are shown in Figure 11. Maximum power densities for all LSCX materials, fuels, and temperatures are summarized in Figures 12−14. The fuel cell performance in CH_4 was the lowest achieved using any of the tested fuels, and there was a rapid reduction in current density starting around 0.5 V. Each of the oxides except for

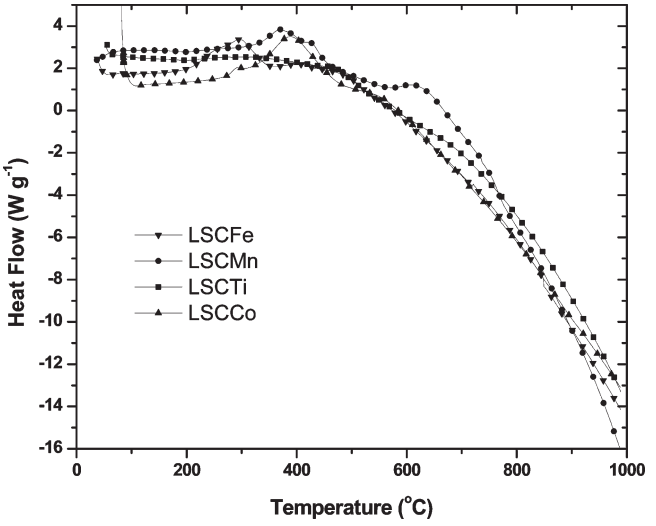

Figure 8. DSC data during TPO of oxide anode materials in 5% O_2.

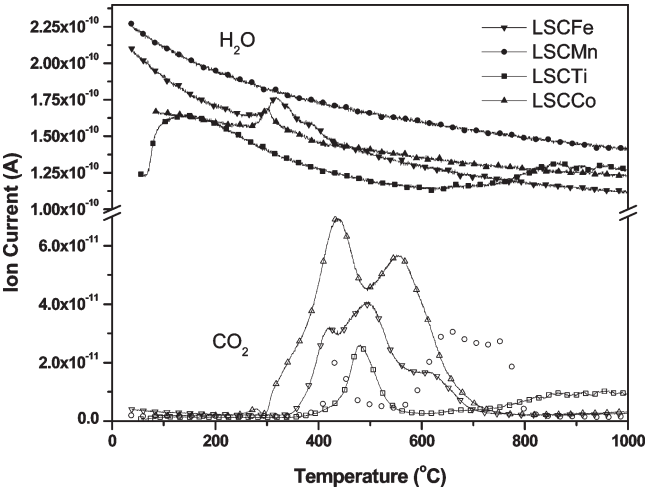

Figure 9. MS data during TPO of oxide anode materials in 5% O_2.

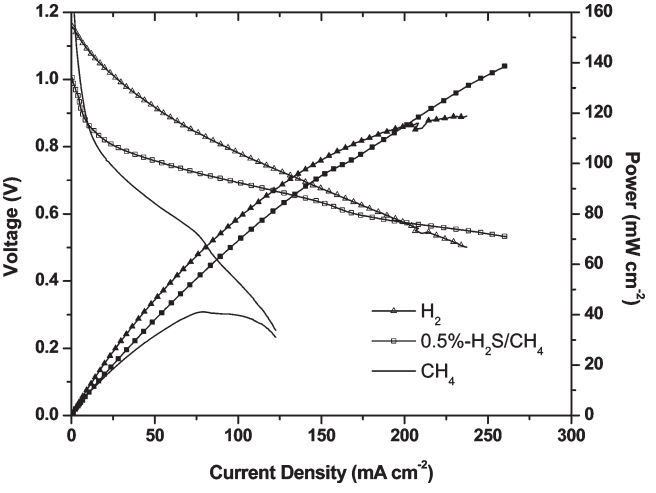

Figure 10. Potentiodynamic curves for LSCFe|YSZ|Pt at 850 °C.

LSCTi performed very well in H_2 (Figure 12). LSCTi showed no apparent activity for activation of either CH_4 or H_2 (Figures 12 and 13). All of the anodes were active in 0.5% H_2S/CH_4 feed (Figure 14). At OCV, the impedance

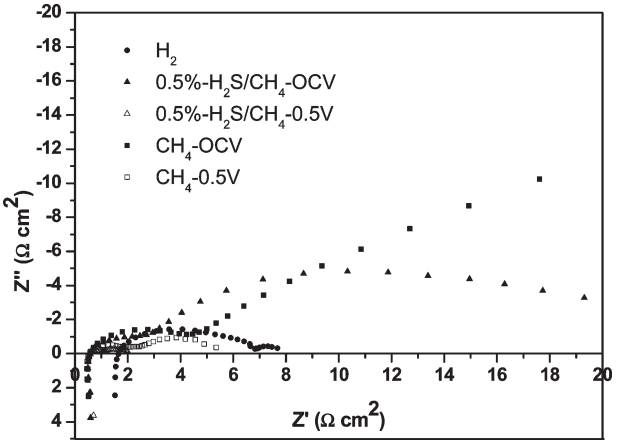

Figure 11. Impedance spectra for LSCFe|YSZ|Pt at 850 °C.

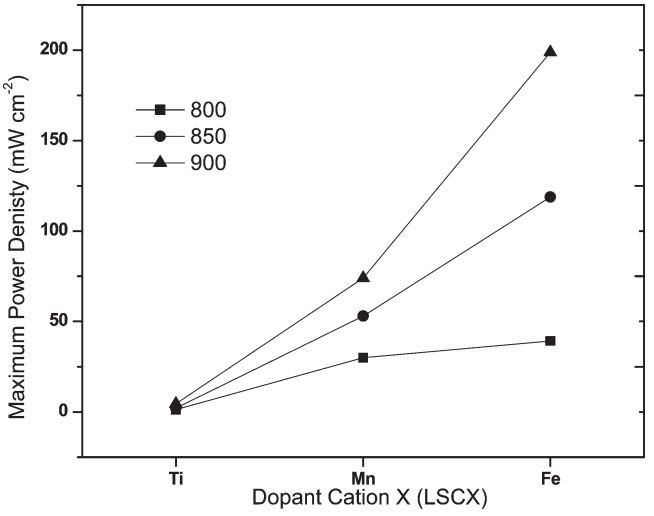

Figure 12. Dependence of performance on substituent cation using H_2 feed.

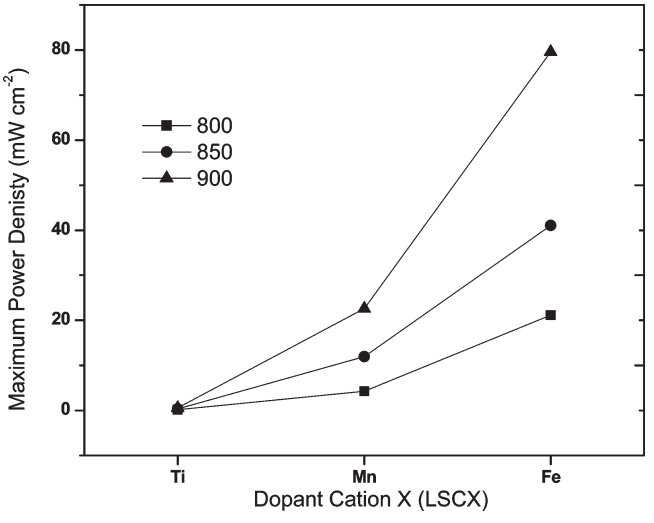

Figure 13. Dependence of performance on substituent cation using CH_4 feed.

curves in H_2 showed low polarization resistance values for each anode, higher values in 0.5% H_2S/CH_4, and very high values in CH_4. In sour gas and CH_4, the polarization

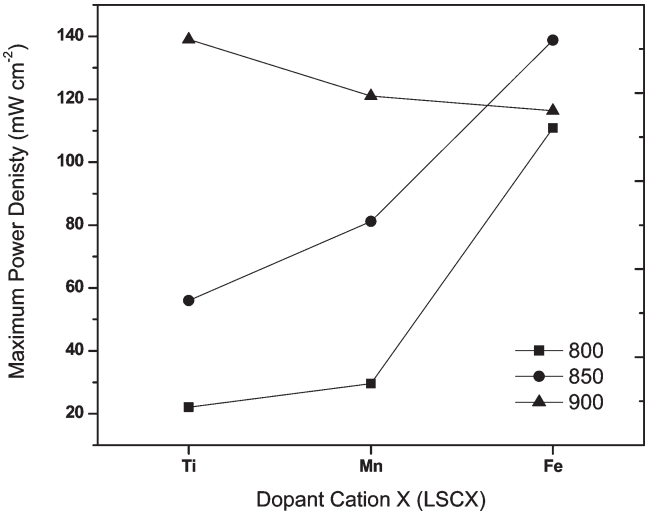

Figure 14. Dependence of performance on substituent cation using 0.5% H_2S/CH_4 feed.

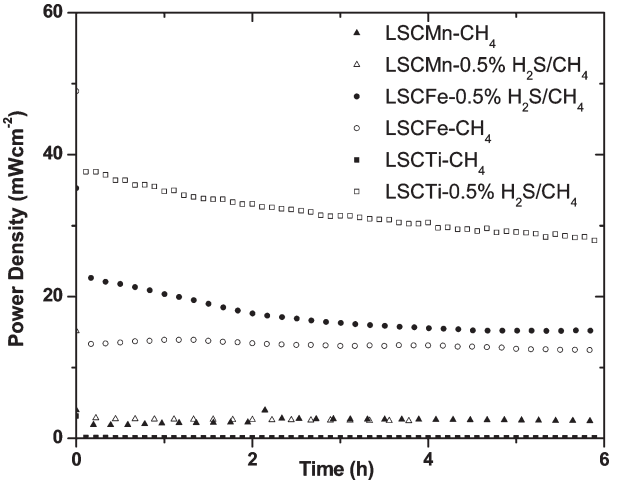

Figure 15. Long-term potentiostatic test at 0.7 V of LSCX|YSZ|Pt at 850 °C.

resistances decreased drastically with the application of overvoltage during impedance measurements. The rankings of the activities of LSCX oxides (X = Ti, Mn, Fe) according to power density values in the different feeds were the following: H_2, Fe > Mn > Ti; CH_4, Fe > Mn > Ti; and 0.5% H_2S/CH_4, Fe > Mn > Ti at 800 °C and 850 °C, and Ti > Mn > Fe at 900 °C.

Potentiostatic tests were conducted in CH_4 and 0.5% H_2S/CH_4 for 6 h (Figure 15). Initially the highest power was achieved by LSCTi in 0.5% H_2S/CH_4; however, there was a significant reduction in performance (ca. 25%) during the 6 h test. The long-term performance of LSCTi in CH_4 was low and stable. While LSCFe had the second highest power output in CH_4, again there was significant reduction (>20%) in performance over 6 h. The performance of LSCFe was stable in 0.5% H_2S/CH_4. LSCMn had similar stable, lower power output in either CH_4 or 0.5% H_2S/CH_4, suggesting that there was little influence from the presence of H_2S in this case.

In an attempt to improve the sinterability of MEA and to enhance anode catalyst activity through introduction

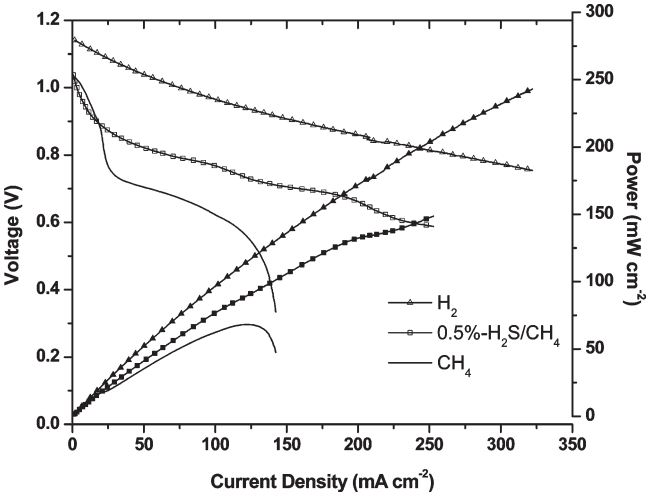

Figure 16. Potentiodynamic curves for LSCFe-GDC|YSZ|Pt at 850 °C.

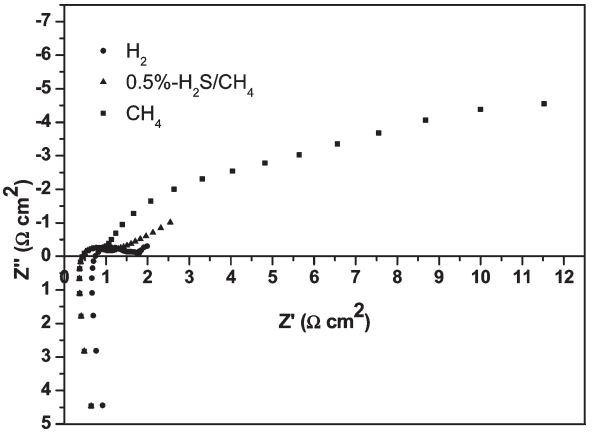

Figure 17. Impedance spectra for LSCFe-GDC|YSZ|Pt at 850 °C.

of complementary capability, we compared performances of composite anodes comprising mixtures of LSCX with GDC. The performances of the composites were in each case superior to those of the single component LSCX anodes at all temperatures. A typical performance curve is shown in Figure 16 for a fuel cell using the LSCFe−GDC composite anode at 850 °C, and the corresponding impedance curve is shown in Figure 17. The maximum power densities for all composite anodes with all feeds are shown in Figure 18. With the addition of GDC to LSCCo, it still was possible to sinter various suitable combinations of anode and electrolyte to form MEAs, even when there was a mismatch of expansion coefficients between the anode and the YSZ electrolyte. The polarization resistances and ohmic resistances of all composite anodes were reduced compared to the corresponding LSCX alone. However, it was found again that there were similar limiting current losses when using CH_4 as a fuel. The highest power densities were achieved using H_2 as a fuel, while in 0.5% H_2S/CH_4 the maximum power density was approximately 50% of that value. The highest power density, almost 250 mW cm^{-2}, was achieved in H_2 using LSCFe−GDC as the anode. The ranking of the LSCX−GDC composite anodes according to maximum power density values using the different fuels was as

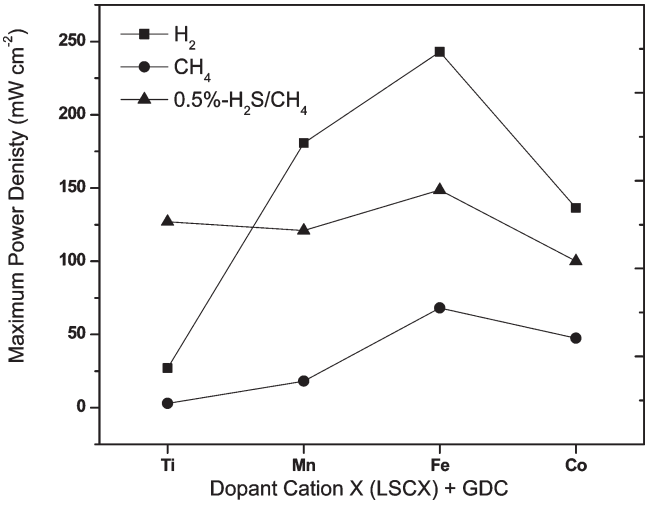

Figure 18. Summary of influence of GDC on performances at 850 °C.

follows: H_2, Fe > Mn > Co > Ti; CH_4, Fe > Co > Mn > Ti; and 0.5% H_2S/CH_4, Fe > Ti > Mn > Co. It is noteworthy that the composite anodes containing LSCCo−GDC were more stable during testing, in contrast to LSCCo alone.

A mass spectrometer was connected to the outlet of the anode compartment of the fuel cell to analyze the effluent gas so as to determine the products formed and thereby gain insight into the process and reaction mechanism. The gas was analyzed before, during a potentiodynamic sweep (0 V to −OCV), and after that sweep. The results for LSCFe−GDC at 850 °C are shown in Figure 19. CO_2 and H_2O were produced when CH_4 was used as a fuel, while the effluent contained CS_2, CO_2, SO_2, and H_2O when 0.5% H_2S/CH_4 was used over all LSCX−GDC composites at all temperatures. The exceptions were LSCCo−GDC which was readily reduced, as described above, and LSCTi which had essentially no activity in pure CH_4, although CO_2 was produced when 0.5% H_2S/CH_4 was used as the fuel.

4.0. Discussion

Conductivity, TEC, and surface area measurements indicated that all four LSCX oxides have comparable structures and physical and electrical properties. The oxides where X = Ti, Mn, or Fe were all stable under reducing conditions, but LSCCo was not, and so, that material was unsuitable for use as a fuel cell anode material.

In conventional TPR, oxygen is fed with methane over a heterogeneous catalyst and the methane oxidation reaction (eq 1) occurs over the surface, as previously performed using LSCFe and LSCMn.[14,28] While there is a correlation between these tests and fuel cell experiments, the test conditions do not truly represent the fuel cell anode environment. In this study, the CH_4 TPR was conducted without cofeeding oxygen, and the oxygen necessary for the methane oxidation reaction was provided from the catalyst, as

(27) Kharton, V. V.; Tsipis, E. V.; Marozau, I. P.; Viskup, A. P.; Frade, J. R.; Irvine, J. T. S. *Solid State Ionics* **2007**, *178*, 101.
(28) Tao, S; Irvine, J. T. S.; Plint, S. M. *J. Phys. Chem. B* **2006**, *110*, 21771.

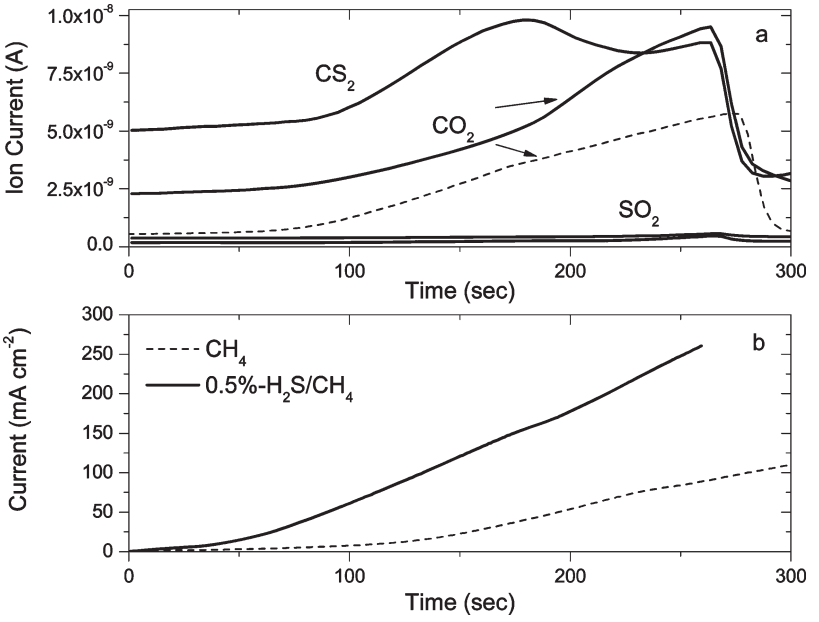

Figure 19. Variation of (a) anodic cell exhaust with (b) cell current for LSCFe|YSZ|Pt at 850 °C.

initially described by Baker and Metcalfe and recently employed by McIntosh.[17,18,24−26] Baker and Metcalfe used a steady state TPR method similar to that used here, while McIntosh used a pulsed TPR technique to examine the effect of oxygen nonstoichiometry on the methane oxidation activity.

$$CH_4 + 2O_2 \rightarrow CO_2 + 2H_2O \quad (1)$$

A good fuel cell catalyst would provide oxygen, replenished by conduction of oxide ions via the electrolyte, while retaining its structure, thereby retaining physical integrity and electrocatalytic activity without risking severance of the bond to the electrolyte. The equivalent electrochemical reaction in the fuel cell is (eq 2).

$$CH_4 + 4O^{2-} \rightarrow CO_2 + 2H_2O + 8e^- \quad (2)$$

The oxides LSCX, X = Ti, Mn, Fe, retained their structure during oxidation of CH_4 and were fully regenerated under O_2. However, LSCCo was not stable under reducing conditions. The TPR tests were conducted after an oxidation−reduction−reoxidation treatment to ensure that no carbonaceous contaminant was present on the surface. The temperature at which the oxidation reaction started to occur and the amount of CO/CO_2 released during TPR was indicative of the capability of the catalyst to activate methane. Three reaction characteristics correlated with good activity of the catalyst: a lower initial reaction temperature, a greater amount of CO/CO_2 released, and a narrower CO/CO_2 peak. The most active oxidation catalysts were those containing cations to the right of Cr in the periodic table: Mn, Fe, and Co. As Mn and Fe were the most active, they appeared to have the highest potential for activity as fuel cell catalysts. Our findings for LSCM are supported by the findings of McIntosh, where they used a similar experimental setup and obtained similar TPR temperatures and MS signals.[17,18]

All of the materials showed signs of coke formation, and the normalized amount of formed coke was similar for all materials. The temperature at which CO_2 was removed during TPO was indicative of the catalyst−coke bond strength. A low temperature for CO_2 evolution indicated that the deposited carbon was easily removed. In contrast, LSCMn had more refractory carbon deposits, since oxidation at 600−800 °C was required to remove the bulk of the coke as CO_2. LSCFe had the least refractory carbon, and the bulk of the CO_2 evolved between 400 and 500 °C. Second, evolution of water at 250−350 °C, as well as DSC peaks corresponding to exothermic heat evolved during the oxidation of carbonaceous deposits intimately bonded to the oxide powder, showed the presence of adsorbed CH_x species on the surface of LSCFe, LSCMn, and LSCCo. Oxidation of the deposits on LSCTi did not produce a peak for H_2O, indicating that carbon was formed by cracking of methane in the gas stream.

Data from electrochemical testing of selected anode materials were in the same order as activities for CH_4 TPR: LSCFe was the most electrochemically active, followed by Mn and Ti. Additionally, CH_4 active catalysts were also active toward H_2 and 0.5% H_2S/CH_4, with a similar ranking in terms of activity. The anodes were most active in either H_2 or H_2S-containing CH_4. However, there was a severe limit on the current density above 0.5 V when CH_4 alone was used as fuel. When a low potential was applied the LSCFe anode was stable in CH_4 fuel but not in 0.5% H_2S/CH_4. LSCMn was stable in both fuels under potentiostatic conditions.

Addition of GDC to form composite anodes improved the oxygen ion conductivity of the anode and expanded the triple phase boundary area of each anode without affecting the order of activity using any of the fuels. By forming a composite of GDC and LSCCo, it was possible to overcome the TEC mismatch, sinter, and test a Co-containing anode for an MEA. LSCCo−GDC was not as active as LSCFe−GDC but was slightly more

active than LSCMn−GDC, characteristic of a volcano type plot for activity when H_2 and CH_4 are used as fuel.[16]

Compositions of MEAs with and without GDC were not optimized for performance; however, the batches of each material were closely replicated for reproducibility of performance, with standard deviation within ±10%. Electrolyte supported cells all had Pt as the cathode, to enable comparison of anode performance.

The difference between performances in CH_4 and H_2S/CH_4 showed that the addition of H_2S changed either or both of the reaction mechanism and the surface state. The MS results revealed information about the process and the possible reaction mechanism occurring in the presence of H_2S. Not only was H_2S electrochemically oxidized (eq 3 and 4), it also appeared to participate in and affect the conversion of CH_4. CS_2 was produced, indicating the possibility that CH_4 first dissociated on the catalyst surface (eq 5), then reacted with surface S (*S) or a S-containing species (eq 6).

$$H_2S + O^{2-} \rightarrow 1/2S_2 + H_2O + 2e^- \quad (3)$$

$$H_2S + 3O^{2-} \rightarrow SO_2 + H_2O + 6e^- \quad (4)$$

$$CH_4 \rightarrow *C + 2H_2 \quad (5)$$

$$*C + 2*S \rightarrow CS_2 \quad (6)$$

This reaction path is thermodynamically viable as reaction 7 has a negative free energy above 600 °C.

$$C + 2H_2S \rightarrow CS_2 + 2H_2 \quad (\Delta G_{850C} = -132\ \text{kJ mol}^{-1}) \quad (7)$$

Alternatively, the sulfur may have provided adsorption sites between the oxide anode surface and CH_4, after which further reactions would form CS_2 (eq 8).

$$*H - S + CH_4 \rightarrow *H - S - CH_4 \rightarrow \text{products} \quad (8)$$

A gas phase reaction between H_2S and CH_4 was unfavorable: the amount of CS_2 in our system would be very low (371 ppm at 850 °C), and the concentration of CS_2 would be dependent of the current drawn from the cell.

Furthermore, there was a greyish film on the surface of all used anodes after being operated potentiostatically, regardless of the anode used. A similar effect was reported for use of 5% H_2S/CH_4 gas on NiS−YSZ and CoS−YSZ anode materials.[29,30] XPS analysis of the surface powder shows the presence of a C−O−S on the surface, with O and S having different binding energies and peaks. TPO of the anode powders showed CO_2 and SO_2 evolution from the surface of the anode. The amount of carbon present was greater than for the anodes tested in pure CH_4. This further indicated participation of S in the anodic reaction. Unfortunately, the present data are insufficient to fully define the reaction mechanism.

(29) Grgicak, C. M.; Green, R.; Giorgi, J. B. *J. Power Sources* **2008**, *179*, 317.
(30) Grgicak, C. M.; Pakulska, M. M.; O'Brien, J. S.; Giorgi, J. B. *J. Power Sources* **2008**, *183*, 26.

5.0. Conclusions

Catalytic and electrocatalytic activities of perovskites $La_{0.75}Sr_{0.25}Cr_{0.5}X_{0.5}O_{3-\delta}$ (LSCX; where X are cations of the early D-transition metals, Ti, Mn, Fe, Co), and their utility as fuel cell anodes using H_2 and H_2S- and CH_4-containing fuels, each depend on the nature of X.

1. The oxides where X = Ti, Mn, Fe were sufficiently conductive for fuel cell anode catalyst applications.
2. However, LSCCo alone was not stable under reducing conditions, and there was a large thermal expansion coefficient mismatch with YSZ.
3. Composite catalysts comprising equal amounts of LSCX and $Ce_{0.9}Ga_{0.1}O_2$ (GDC) were each more active than the corresponding LSCX alone, due at least in part to the additional ionic conductivity imparted by the mixed conductor GDC. Further, GDC stabilized LSCCo sufficiently to enable its use as anode catalyst.
4. Temperature programmed reaction (TPR) of CH_4 under O_2-free conditions showed that the catalytic activity of the oxides for conversion of CH_4 was in the order Co > Mn > Fe > Ti.
5. The order of CH_4 TPR activities of LSCX was approximately parallel with their electrocatalytic activity. Thus, TPR was useful as a preliminary predictor of electrocatalytic activity for conversion of CH_4, which was found to be Fe > Mn > Ti for LSCX alone and Fe > Co > Mn > Ti for LSCX−GDC.
6. Fuel cell performance using each of LSCX was highest using H_2 fuel and lower using CH_4. When the fuel was 0.5% H_2S/CH_4, the performance was considerably greater than that in CH_4 alone and close to that when using pure H_2. Fuel cells using anodes LSCX−GDC performed considerably better than those using LSCX alone; the highest performance attained was 250 mW cm^{-2} using a fuel cell with the configuration LSCFe−GDC|YSZ (0.3 mm)|Pt at 850 °C.
7. The composition of the effluent streams during fuel cell tests, determined using in situ MS, varied with LSCX. The effluent when 0.5% H_2S/CH_4 was used as a feed differed from that from sulfur-free feeds, and CS_2 was present in the effluent.

Acknowledgment. This research was supported through funding to the NSERC Solid Oxide Fuel Cell Canada Strategic Research Network from the Natural Science and Engineering Research Council (NSERC). The authors would like to thank S. Merali (XRD), M. Danaie (SEM), D. Karpuzov and A. He (XPS), B. Shalchi (BET), and S. Yick (Dil.) for assistance with instrumental methods for characterization of materials.